AIAA JOURNAL
Vol. 34, No. 7, July 1996

Unsteady Aerodynamic Model of Flapping Wings

Michael S. Vest* and Joseph Katz†
San Diego State University, San Diego, California 92182-1308

Propulsive forces can be generated with flapping or heaving wings traveling through a fluid, as demonstrated in animal flight. To examine the flowfield around variable geometry bodies, with specific application to the unsteady flow associated with flapping wings, an unsteady, three-dimensional, incompressible, potential flow model was developed. The problem is formulated in an inertial reference frame such that the body moves through an otherwise quiescent fluid. Results were compared with the limited experimental results available and analytical methods. In one case the model was applied to a flapping wing in a wind tunnel at high advance ratios ($J = 4.31$) where the computed average lift and thrust were within the error bounds of the experimental data. The model was also applied to high-frequency flapping flight ($J = 0.76$) of a pigeon flying in a wind tunnel, where the predicted lift matched the weight of the bird.

Nomenclature

A, B = influence coefficients [Eqs. (11) and (12)]
AR = aspect ratio, $(b_{\text{ref}}^2/S_{\text{ref}})$
b = wing span
C_D = drag coefficient, $[D/(\frac{1}{2}\rho V_{\text{ref}}^2 S_{\text{ref}})]$
C_L = lift coefficient, $[L/(\frac{1}{2}\rho V_{\text{ref}}^2 S_{\text{ref}})]$
C_P = power coefficient, $[P/(\frac{1}{2}\rho V_{\text{ref}}^3 S_{\text{ref}})]$
C_p = pressure coefficient [Eq. (15)]
C_T = thrust coefficient, $(-C_D)$
c = wing chord
$\boldsymbol{F}$ = fluid dynamic force vector
f = natural frequency
J = advance ratio, $[2V_{\text{ref}}/(b_{\text{ref}}\phi_1\omega_\phi) = 1/(b_{\text{ref}}^*\phi_1 k_\phi)]$
K_α = twist coefficient [Eq. (23)]
k_ϕ = reduced flapping frequency, $(\omega_\phi c_{\text{ref}}/2V_{\text{ref}})$
$\boldsymbol{M}$ = fluid dynamic moment vector
m = mass of pigeon
N = number of panels
$\boldsymbol{n}$ = normal vector
P = power
P_{in} = input power
P_{out} = output power
P_{par} = parasitic power
P_{pro} = profile power
p = pressure
$\boldsymbol{R}$ = position vector in space-fixed system
Re = Reynolds number
$\boldsymbol{r}$ = position vector in body-fixed system
S = surface area
T = thrust
t = time
$\boldsymbol{V}$ = velocity vector
α = angle of attack
β = phase shift
Γ = circulation
$\gamma_{T.E.}$ = change in streamwise circulation at the trailing edge of the body
γ_W = strength and orientation of circulation in wake
η = flight efficiency [Eq. (20)]
Θ = rotation vector $\langle\phi, \theta, \psi\rangle$
θ = rotation about the Y axis
μ = doublet strength—jump in potential across surface
ρ = fluid density
σ = source strength—jump in normal component of velocity across surface
τ = downstroke ratio
Φ = total velocity potential
ϕ = rotation about the X axis
ψ = rotation about the Z axis
Ω = rotation rate vector $(\dot{\Theta})$
ω_ϕ = flapping circular frequency $(2\pi f_\phi)$

Subscripts and Superscripts

B = body
i = collocation point counter
j = body panel counter
k = wake panel counter
ref = reference conditions
$T.E.$ = trailing edge
t = twist
W = wake
$\Delta()$ = increment due to panel
0 = body-fixed system with respect to space-fixed system
∞ = freestream conditions far from body
$'$ = per unit span
$*$ = nondimensionalized

Introduction

PROPULSION systems of conventional aircraft and watercraft (e.g., propellers, rotors, turbines) are characterized by continuous cyclic motion with only a few exceptions. The physiology of aquatic propulsion and animal flight, however, is dominated by harmonic, reciprocating motions. Because of this unsteady motion, traditional aerodynamic theory based on steady or quasisteady aerodynamic assumptions may be inadequate in modeling some aspects of animal aerodynamic and propulsive mechanisms.

Because of the reciprocating motions involved, the analysis of avian flight is probably one of the more complex aerodynamic problems examined. The analysis is complicated by the many unique capabilities of a bird. Simplifications in both the fluid dynamic model and the geometry of the body must be made if any kind of insight into the characteristics of flapping wings is hoped to be accomplished. A review of various flapping wing models can be found in Ref. 1. The techniques currently used for avian flight can essentially be divided into three steady or quasisteady methods: momentum jet (actuator disk) and blade element theories,[2] lifting line theory,[3,4] or a vortex ring theory.[5]

The propulsive force derived from the flapping motion can be seen in Fig. 1. From the Kutta–Joukowski theorem[6] ($\boldsymbol{F}' = \rho \boldsymbol{V} \times \Gamma$) we

Presented as Paper 95-0747 at the AIAA 33rd Aerospace Sciences Meeting, Reno, NV, Jan. 9–12, 1995; received March 11, 1995; revision received Aug. 9, 1995; accepted for publication Aug. 14, 1995.

*Graduate Student, Department of Aerospace Engineering and Engineering Mechanics. Student Member AIAA.
†Professor, Department of Aerospace Engineering and Engineering Mechanics. Associate Fellow AIAA.

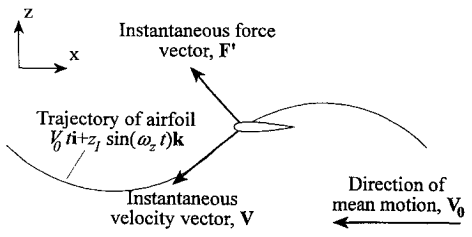

Fig. 1 Description of propulsive forces generated by the heaving motion of an airfoil.

can see that the force per unit span produced by a two-dimensional airfoil undergoing heaving oscillations will produce a forward-oriented force vector, based on the instantaneous velocity of the airfoil. This instantaneous velocity is composed of mean forward translational motion and vertical heaving motion components. When integrated over the heaving cycle, a net thrust force is produced by the motion of the airfoil. For a symmetric airfoil at zero incidence (relative to the mean direction of motion), the average lift will be zero, but there will be a periodic thrust in the direction of mean motion. If the amplitude of the heaving motion is such that the thrust produced is greater than the drag of the wing/body system, then the system will be accelerated in the direction of motion.

Because of the unsteady motion of the body, the wake created behind the body will be inherently unsteady. Phlips et al.[3] also demonstrated the importance of accurate modeling of the unsteady wake behind the flapping wing. Depending on the advance ratio, the strength and location of this wake will influence the forces on the body. Therefore an appropriate model of the wake is essential in predicting the aerodynamics of the body. For example, Rayner's vortex theory of animal flight[5] is based on the wake being formed by a series of vortex rings being periodically shed into the wake. Flow visualization of the wake behind a bird[7,8] shows that this model is not quite realistic based on the circulation of the visualized wake; the momentum of the vortex rings produced less than 35% of the momentum necessary to support the weight of the bird.

The best approach would be to solve the complete viscous flow near the bird. However, solution of the full Navier–Stokes equations for three-dimensional, unsteady flowfields are challenging to solve, and for the flow around variable geometry bodies this problem is complicated even further. Another popular method that is available to compute the unsteady flow about arbitrary bodies is the potential flow panel method. A review of the various panel methods can be found in Ref. 6. Recently[9,10] these methods have been used to model unsteady flows with encouraging results. In the current model, the motion of the body is known (prescribed). The problem is formulated in a space-fixed (inertial) reference frame unlike most previous methods that are formulated in a body-fixed (wind tunnel) coordinate system. This will ease the computational effort when examining the wake and the interaction of several bodies or body patches. Each wing is assumed solid and rotates about a common axis. By using a time-stepping solution procedure, the shape of the trailing wake will be determined from the calculations. This model is unique in its ability to handle a time-dependent deformable body such as flapping wings.

Fluid Dynamic Model

For the bodies mentioned here, the flow is dominated by the inertial terms in the Navier–Stokes equations (i.e., aircraft: $Re \approx 10^7$, birds: $Re \approx 10^5$), and the viscous effects are confined to regions near the body and the wake shed behind the body. In the cases considered, the majority of the flowfield behaves as an inviscid flow. Since most vorticity production is caused by viscous stresses, vorticity will be confined to the boundary layer and wake, and outside of this region the flow is assumed irrotational. Provided that the body is sufficiently streamlined so that the flow does not separate from the body, the viscous region will be thin. If the body is traveling at low speeds (much slower than the speed of sound) through a homogeneous fluid, then the flow can also be assumed incompressible. The trailing wake is also assumed to be deformable and force free. With these assumptions, the solution of the flowfield can be divided into

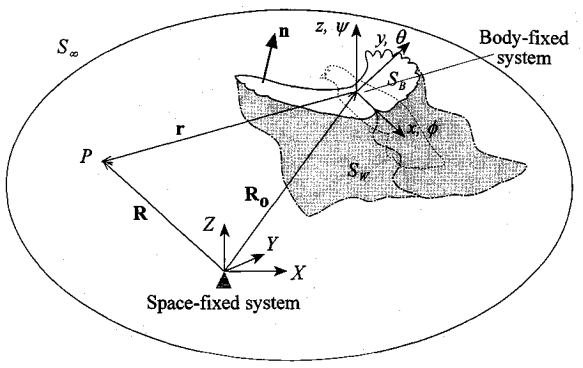

Fig. 2 Schematic of representative flowfield.

two parts. First, solve the inviscid problem for the external pressure and velocity field. Then, from the inviscid results, solve the inner viscous solution. The purpose of this study is to examine the inviscid external flowfield only. This will give a good estimation of the pressure forces on the body (resulting in engineering information such as lift, induced drag, etc.) but does not account for the skin friction or separation (form) drag. If these viscous forces are important, a more robust analysis of the viscous region must be performed.

Governing Equation

For the proposed flowfield, the potential flow is governed by Laplace's equation,

$$\nabla^2 \Phi = 0 \tag{1}$$

It can be seen from Eq. (1) that the velocity potential for an incompressible, irrotational fluid must satisfy Laplace's equation at every point in space. Equation (1) governs the velocity potential variation throughout the flowfield, but it doesn't give any information on the flow evolution in time; the temporal dependency must be introduced through the boundary conditions. In general, the motion of the body depends on the dynamic and fluid mechanic loads. For this study, however, the body kinematics are prescribed and the fluid dynamics loads are computed from this prescribed motion.

Boundary Conditions

Since Eq. (1) is elliptic, the boundary condition must be specified on all surfaces bounding the flow. For a body moving with respect to a space-fixed reference frame through an otherwise quiescent fluid (Fig. 2), the far-field boundary condition can be stated such that any disturbance caused by the body must decay far from the body and wake:

$$\lim_{r=|R-R_0|\to\infty} \nabla\Phi = 0 \tag{2}$$

Also, since the body is assumed to be solid, the velocity normal to its surface must be zero:

$$\boldsymbol{V}\cdot\boldsymbol{n} = [\nabla\Phi(\boldsymbol{r},t) - \boldsymbol{V}_{\text{Surface}}(\boldsymbol{r},t)]\cdot\boldsymbol{n}(\boldsymbol{r},t) = 0 \tag{3}$$

This surface velocity is given as

$$\boldsymbol{V}_{\text{Surface}}(\boldsymbol{r},t) = \boldsymbol{V}_0(t) + \Omega(t)\times\boldsymbol{r}(t) + \boldsymbol{v}_{\text{Relative}}(\boldsymbol{r},t) \tag{4}$$

where $\boldsymbol{v}_{\text{Relative}}$ accounts for any relative motion of the surface (secondary motions, porosity, blowing, etc.) within the body-fixed system.

Physical Considerations—Vortex Wake

As stated previously, all vorticity is assumed to be confined to the boundary layer on the surface of the body and in a thin vortex wake shed behind the body. In addition to computing the circulation produced by the body, the circulation and shape of this wake must be determined.

The time dependency in the problem is introduced through Eqs. (3) and (4). An additional constraint on the temporal evolution of the flowfield is introduced by Kelvin's theorem, which states that the total circulation around a fluid curve remains constant,

$$\frac{d\Gamma}{dt} = \frac{d\Gamma_B}{dt} + \frac{d\Gamma_W}{dt} = 0 \tag{5}$$

Therefore any change in circulation around the body will be balanced by a change in circulation of the wake.

An additional physical limitation needs to be imposed at the trailing edge to fix the circulation on the wing. A popular choice is to use the Kutta condition that states that the velocity must leave the sharp trailing edge smoothly and that the velocity there is finite. One possible interpretation of this condition is to fix the circulation along the trailing edge such that[2,6]

$$\gamma_{T.E.} = 0 \tag{6}$$

The preceding conditions hold well if the kinematic velocity normal to the trailing edge is much smaller than the translational velocity. For unsteady flows with high reduced frequencies, the classical Kutta condition probably is not an acceptable condition. Experiments[11–13] have shown that for high reduced frequency flows, in the region of the trailing edge the flow departs significantly from that expected from the steady Kutta condition. Satyanarayana and Davis[12] noted that this departure affects the pressure in the region of the trailing edge and may not affect the unsteady lift, but contribution to the pitching moments will be great. Giesing[14,15] suggests that the flow will leave the trailing edge parallel to the upper or lower surfaces of the trailing edges of the airfoil depending on the rate of circulation shed from the body. Basu and Hancock[16] suggest a different method for calculating the angle at which the flow leaves the trailing edge. Poling and Telionis[13] show that an airfoil is loaded in a region 3–5% of the wing chord behind the airfoil and the pressure jump there is about 10% of the mean C_p of the airfoil due to strong viscous interactions of the boundary layer of the airfoil. They noticed that the flow leaves the trailing edge at the Giesing angles (i.e., parallel to one edge of the airfoil) and moves smoothly from one edge to the other for small changes in circulation ($\Gamma_B \approx$ const). In the present model the flow is assumed to leave the trailing edge along the bisector and then follows the local stream direction.

The wake deformation is obtained by assuming it to be force free, and so the pressure difference across the wake must be zero. Therefore,

$$\Delta \boldsymbol{F} = \Delta S \rho \boldsymbol{V} \times \boldsymbol{\gamma} = 0 \tag{7}$$

Except for the trivial case when the circulation or velocity of the wake is zero, this equation can only be satisfied when $\boldsymbol{V}_W$ is parallel to γ_W, or

$$\boldsymbol{V}_W \| \gamma_W \tag{8}$$

This condition can be met by moving the wake to a force-free position at every time step.

Solution of Laplace's Equation

The solution of Eq. (1), subject to the boundary conditions [Eqs. (2) and (3)], can be found using Green's second identity that expresses the solution in terms of source and doublet singularities distributed over the surface of the body and its wake. Since the problem is formulated in a space-fixed reference frame (Fig. 2), the potential contribution on the far-field boundary S_∞ is zero, and so the total velocity potential at any point in the interior or exterior flowfield can be found from[6]

$$\Phi(\boldsymbol{r}, t) = \iint_{S_B} \left(\frac{\sigma}{4\pi r} - \mu \frac{\partial}{\partial n} \frac{1}{4\pi r} \right) dS - \iint_{S_W} \left(\mu \frac{\partial}{\partial n} \frac{1}{4\pi r} \right) dS \tag{9}$$

There are many combinations of source and doublet strengths that will yield a solution to Eq. (9). One possible choice[6,9,10] is to set the internal potential on S_B such that $\Phi_{\text{Internal}} = 0$. Note that the inertial frame is attached to the undisturbed fluid and the traditional perturbation potential becomes the total potential. Also, the potential jump on S_B becomes $-\mu$, whereas the boundary condition [(Eq. (3)] for the velocity jump across S_B sets the source strength

$$-\sigma = \boldsymbol{n} \cdot \nabla \Phi = \boldsymbol{n} \cdot \boldsymbol{V}_{\text{Surface}} \tag{10}$$

Thus, the source strengths are known from the prescribed motion. The only unknowns then are the doublet strengths (or external potential) on the body. From Eq. (9) the velocity potential at any point in the flow can be found from the external potential μ on the surface of the body and wake.

The integration over the body can be broken up into distinct panels and the effect of each panel can be summed. By assuming a constant source and doublet strengths over the small panel element, the singularities can be taken out of the integration. The discretized form of Eq. (9) can now be evaluated at some point $\boldsymbol{r}_i$ on the inside of the body surface S_B where $\Phi_{\text{Internal}} = 0$, and so

$$\Phi(\boldsymbol{r}_i, t) = \sum_{j=1}^{N_B} \mu_j \left[\iint_{S_j} \frac{\partial}{\partial n} \left(\frac{1}{4\pi r_i} \right) dS \right] + \sum_{k=1}^{N_W} \mu_k \left[\iint_{S_k} \frac{\partial}{\partial n} \left(\frac{1}{4\pi r_i} \right) dS \right] + \sum_{j=1}^{N_B} \sigma_j \left[\iint_{S_j} \frac{-1}{4\pi r_i} dS \right] = 0 \tag{11}$$

or in terms of the influence coefficients A and B (which are obtained by the integration on each panel) the algebraic equation

$$\sum_{j=1}^{N_B} \mu_j A_{ij} + \sum_{k=1}^{N_W} \mu_k A_{ik} + \sum_{j=1}^{N_B} \sigma_j B_{ij} = 0 \tag{12}$$

The integration of the influence coefficients A and B depend on the location of the source or doublet panel (indices j or k) and the collocation point (index i) where the potential is being evaluated. The influence coefficients depend solely on the geometry of the problem and are therefore known from the prescribed motion. The source strengths on the body and wake doublet strengths (except for the most recent wake panel) are known. These known values can be placed on one side of the equation and Eq. (12) can be evaluated at each collocation point i (located at the center of each panel) on the body. This gives a set of N_B linear algebraic equations for the $N_B + N_{T.E.}$ unknowns. The additional $N_{T.E.}$ equations come from applying the Kutta condition [Eq. (6)] at each of the $N_{T.E.}$ spanwise trailing-edge wake panels. Reference 6 shows that an equivalent form of Eq. (6) expressing the wake doublet strength in terms of doublet strengths on the upper and lower surfaces of the trailing edge of the wing as

$$\mu_W = \mu_{\text{Upper}} - \mu_{\text{Lower}} \tag{13}$$

This can be evaluated at each of the $N_{T.E.}$ spanwise trailing-edge wake panels, thereby supplying the same number of equations as unknowns.

The solution procedure for the initial value, time-stepping problem is as follows. The body is moved by one time step along the prescribed path. Vortex wake panels are attached to the user-identified trailing-edge panels. Equations (12) and (13) are then solved numerically for the $N_B + N_{T.E.}$ unknowns. For the next time step, the body is moved and the wake location is updated. This wake roll-up is done by computing the velocity induced on each wake panel corner point from all body and wake panels. To model the vortex core, if a given point is within a small cutoff distance of a panel, then the panel contribution is neglected. Each wake point can then be moved using a simple Euler method,

$$\Delta \boldsymbol{R}_W = \boldsymbol{V}_W \Delta t \tag{14}$$

This procedure is repeated for each time step.

As the body motion evolves, for each time step the source and doublet strengths on the body can be found. These can be substituted into Eq. (9) to compute the potential at any point in the fluid. The gradient of the potential will yield the velocity, from which the pressures can be computed using the unsteady Bernoulli equation[6]:

$$(C_p)_i = \frac{p_i - p_0}{\frac{1}{2}\rho V_0^2} = 1 - \frac{V_i^2}{V_0^2} - \frac{2}{V_0^2}\frac{\partial \Phi_i}{\partial t} \tag{15}$$

Likewise the force and moment contribution from each panel can be computed:

$$\Delta \boldsymbol{F}_i = -(C_p)_i\left[\tfrac{1}{2}\rho V_0^2 \Delta S_i\right]\boldsymbol{n}_i \tag{16}$$

and

$$\Delta \boldsymbol{M}_i = \boldsymbol{r}_i \times \Delta \boldsymbol{F}_i \tag{17}$$

These can be integrated over the surface of the body to find the total force and moment on the body.

The input power is simply the power exerted by the muscles to move the wing about the shoulder, or

$$P_{\text{in}}(t) = \sum_{i=1}^{N_B} \Omega \cdot \Delta \boldsymbol{M}_i \tag{18}$$

The output power from the wing is the power used to propel the body through the air, or

$$P_{\text{out}}(t) = \boldsymbol{F} \cdot \boldsymbol{V}_0 + P_{\text{par}} + P_{\text{pro}} \tag{19}$$

where both P_{par} and P_{pro} arise from viscous effects[5] and are unaccounted for in this model. The flight efficiency is the ratio of the output to input powers averaged over a flapping cycle:

$$\bar{\eta} = \frac{\overline{P_{\text{out}}}}{\overline{P_{\text{in}}}} = -\frac{\overline{TV_0}}{\overline{P_{\text{in}}}} = -\frac{\overline{C_T}}{\overline{C_P}} \tag{20}$$

Kinematics Model

Differences in the periods of the up and downstrokes can be accounted for in the downstroke ratio τ, which is the percentage of the total stroke period spent on the downstroke. For the current study, however, the upstroke and downstroke times are assumed to be equal (i.e., $\tau = 0.5$).

A typical geometry of a flapping wing using this model can be seen in Fig. 3. The axis about which the wing flaps is inclined at an angle $\theta(V_0)$ to the freestream velocity. This axis varies with freestream velocity, lying parallel to the freestream air at high flight speeds and becoming perpendicular to the freestream as the bird approaches hovering flight.[2] The origin of the body-fixed system is located at the shoulder since, in a real bird, this would be the point about which all flapping and pitching motions would take place. The instantaneous flapping angle is given by

$$\phi(t) = \phi_0 + \phi_1 \sin(\omega_\phi t + \beta_\phi) \tag{21}$$

The angle of attack of each section chord with respect to θ is given by

$$\alpha(y, t) = \alpha_0 + \alpha_1 \sin(\omega_\alpha t + \beta_\alpha) + \alpha_t(y, t) \tag{22}$$

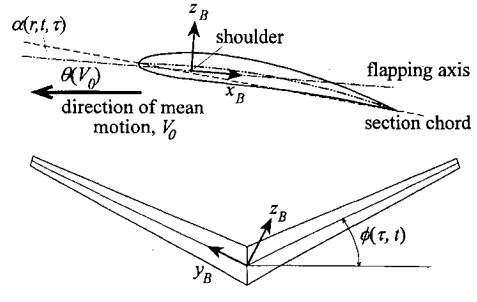

Fig. 3 Representative motions of a flapping wing.

For the current study, α_0 and α_1 are zero, and so only wing twist is examined. Any velocity variations due to α would be accounted for in the v_{Relative} term in Eq. (4).

Results

The methods and procedures just described were incorporated into a computer code that, though developed specifically to handle unsteady three-dimensional flows about variable geometry bodies (such as flapping wings), is capable of computing other flows with minor modifications. Once the code was developed, it was validated against existing steady and unsteady theoretical and experimental data. The model compares well with the steady experimental results[17] of several NACA airfoils in the attached flow regime.

Next, comparisons were made with classic impulsively started wings, both of infinite[18] and finite[19] aspect ratio. The results of the lift and drag for the finite aspect ratio case ($AR = 6$) can be seen in Fig. 4. The steady-state portion of Bernoulli's equation agrees well with the analytic[19] results. A noticeable difference between the $AR = 6$ and $AR = \infty$ cases are that the steady-state lift is less than for the infinite plate. Also, the drag does not approach zero but approaches a finite value. This is the induced drag (drag due to lift) and compares well with the classical steady-state aerodynamic result $C_D \approx C_L^2/\pi AR$ at large t. Figure 5 shows the wake behind

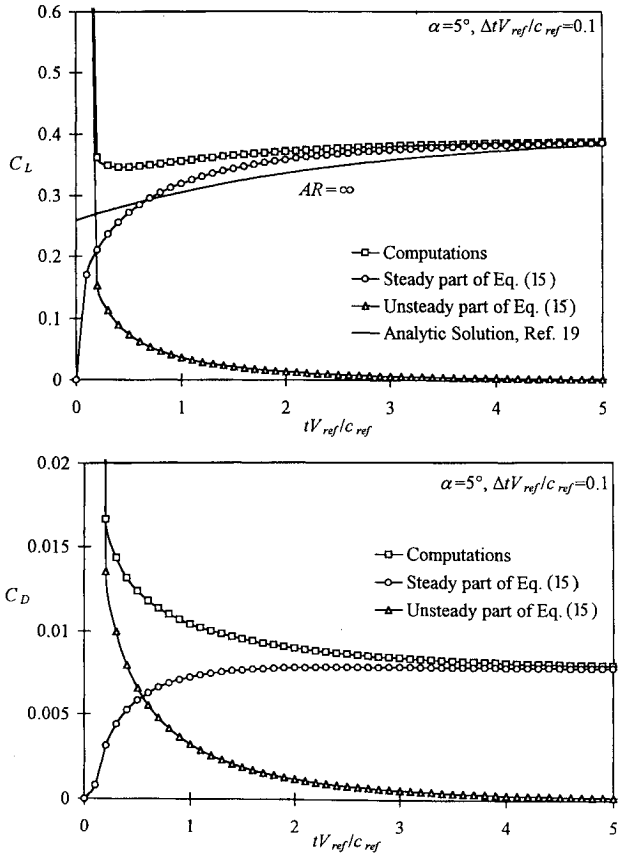

Fig. 4 Lift and drag coefficients for an $AR = 6$ impulsively started flat plate.

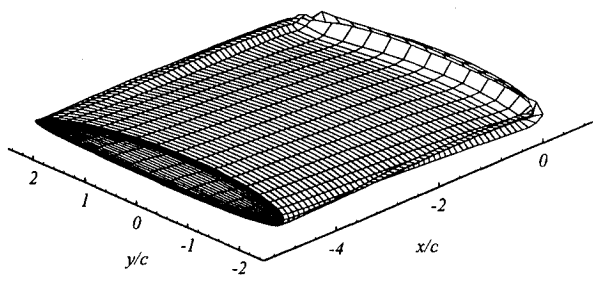

Fig. 5 Wake of an $AR = 6$ impulsively started flat plate.

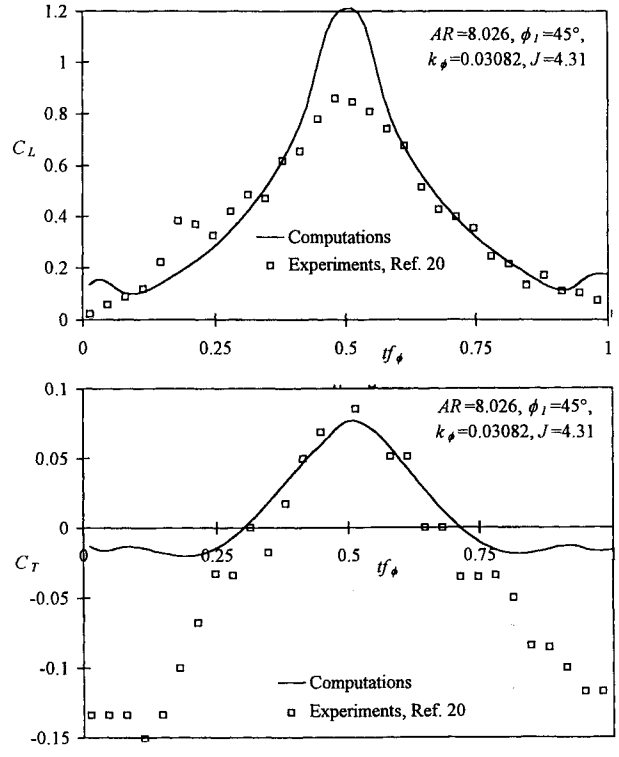

Fig. 6 Lift and thrust coefficient for one flapping cycle of a NACA 8318 wing.

the wing after it has traveled five chord lengths. The code predicts the roll-up of the starting and trailing vortices, which can be seen clearly.

Low-Frequency Flapping Flight

Time-dependent experimental data for flapping wings are virtually nonexistent. It is challenging to design an apparatus to flap wings at the high frequencies experienced by birds in nature. Fejtek and Nehara[20] examined a NACA8318 rectangular wing ($AR = 8.026$) flapping at low frequencies ($k_\phi = 0.03082$) in a wind tunnel. This is representative of a large bird traveling at high speeds (i.e., near gliding speeds). In fast forward flight the flapping motions are generally small and the vertical velocity produced by the flapping motion is much lower than the freestream velocity.

The current model was compared with these wind-tunnel time-dependent force measurements of a flapping wing.[20] As can be seen in the time-dependent lift and thrust curves (Fig. 6), the results agree quite well. On portions of the stroke where the flapping velocity is the greatest, there is some discrepancy between the experimental and computed loads. This effect is most likely due to flow separation on the original experimental wing, creating drag during the upstroke. However, the average loads over a flapping cycle are within errors of the experiment.

High-Frequency Flapping Flight

For the previously mentioned wind-tunnel experiment the flow conditions are quasisteady, and previous avian flight models[2–4] could be used to predict the loads with reasonable accuracy. However, with slow forward flight, the magnitude of flapping is greater and the frequency increases. Because of this high flapping rate, large-amplitude motion, the assumptions of quasisteady theories begin to fail. The maximum vertical velocity (i.e., wing tip speed) is now of the same order as the forward speed. For such a flight condition, the unsteadiness of the problem plays an increasing role in the aerodynamics of the problem.

To study the aerodynamics of flapping wings in slow forward flight, the geometry of a pigeon's wing was chosen. Wing cross-sectional data from Ref. 21 were used as the input geometry for the current model. The resulting wing is shown in Fig. 7. Kinematic and morphological characteristics vary with each individual bird, but typical characteristics of a pigeon that were used in this analysis

Table 1 Kinematic data for a typical pigeon

$c_{ref} = c_{root} = 0.11$ m	$V_0 = V_{ref} = 11$ m/s
$b_{ref} = 0.66$ m $= 6c_{ref}$	$f_\phi = 8$ Hz ($k_\phi = 0.25$)
$S_{ref} = 0.062$ m$^2 = 5.2c_{ref}^2$	$\phi_1 = 50$ deg
$AR = 7.2$	$m = 0.39$ kg

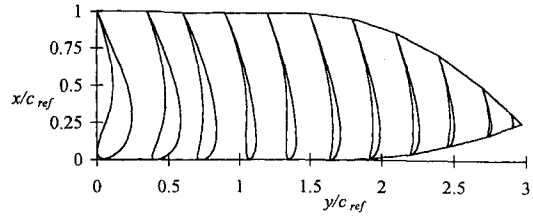

Fig. 7 Cross section of model of pigeon wing.

are given in Table 1. For a first examination of this regime of flight, the wing was assumed rigid.

Without wing twist, the pressure distributions during the downstroke generate a high suction peak near the leading edge. This will inherently cause the flow to separate, which is both undesirable for the bird because of the increase in form drag and violates the assumption of this model that the flow remains attached. This pressure peak becomes more problematic towards the wing tip where the maximum tip velocity is 1.3 times the forward velocity. These large motions of the trailing edge of the wing near the wing tip will also violate the Kutta condition. From both a physical and modeling point of view, this flapping condition is not acceptable.

From photographic analysis of a pigeon in slow flight,[22] it can be seen that the wing twists throughout the wing stroke. To more accurately model the aerodynamics of bird flight, dynamic twisting of the bird's wing was included. To reduce the effects of the large-scale motions near the wing tips, the wing is allowed to twist linearly along the wing from the body towards the wing tip. By doing this the wing is more closely aligned with the instantaneous incoming velocity, keeping the angle of attack with respect to the instantaneous incoming velocity of each spanwise chord at a small angle. The dynamic twist now takes the form

$$\alpha_t(y, t) = K_\alpha \dot{\phi}(t) y \tag{23}$$

where K_α is a constant that allows the magnitude of the pitch oscillations to be adjusted. If this coefficient is set equal to 0.7, then the wing tip twists in such a way that the instantaneous oncoming velocity is always oriented the same way with respect to the section chord. Note that from Eq. (23) the twist angle leads the flapping angle due to the dependency on the flapping velocity.

The effect of both the flapping frequency and the twist coefficient on pressures, loads, power, and flight efficiency can then be examined. Figure 8 shows the average flight efficiency for various pitching amplitudes and flapping frequencies. As expected, for low-frequency (high advance ratio) flight, pitching is not required to keep the flow attached and the highest flight efficiency is obtained with the twist coefficient set to zero. As the flapping frequency is increased, increasing the twist coefficient increases flight efficiency to a point and then, when the pitching magnitude becomes too large, actually causes a loss of efficiency.

Based on the kinematic parameters given in Table 1 for a pigeon flying in a wind tunnel,[22] the reduced flapping frequency chosen by the bird is about $k_\phi = 0.25$ ($J = 0.76$). From Fig. 8, it can be seen that the highest flight efficiency is obtained when the twist coefficient is set to $K_\alpha = 0.6$. For this frequency and wing twist, the average lift coefficient is $\overline{C_L} = 0.85$ and the average thrust coefficient is $\overline{C_T} = 0.13$. Based on the mass of the bird, the lift coefficient required to support the weight of the bird is $C_L = 0.84$, which is almost identical to the average lift coefficient predicted by this model. Form and body drag estimates, based on Ref. 5, give a body drag coefficient of about $C_D = 0.03$ and a wing skin-friction drag of about $C_D = 0.04$. The average thrust produced is still in excess of this and is probably balanced by some flow separation or form drag not predicted by Rayner's drag model, or the bird is

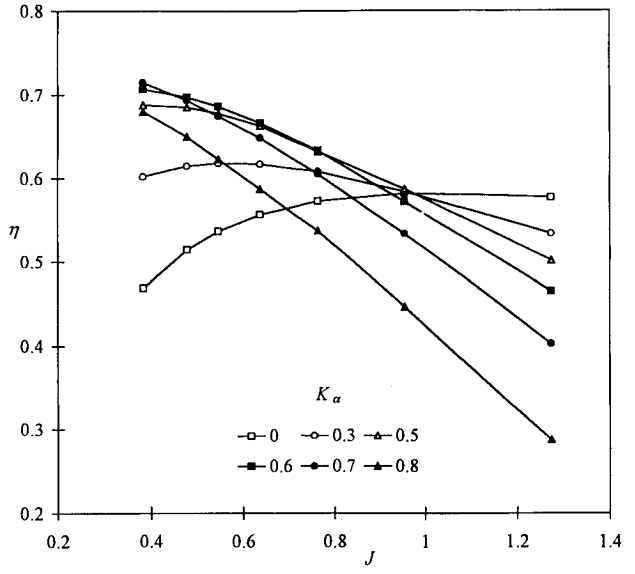

Fig. 8 Flight efficiency for various advance ratios and twist coefficients.

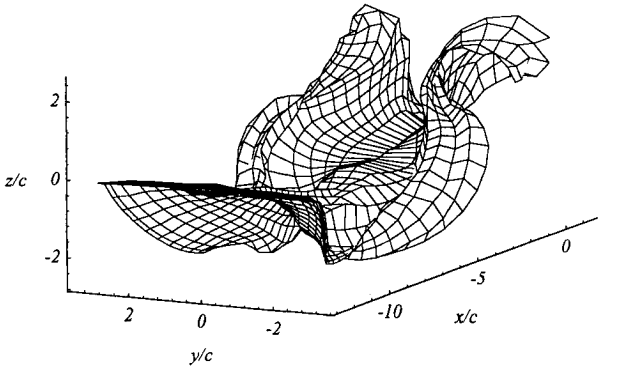

Fig. 9 Pigeon wing and wake for one complete flapping cycle.

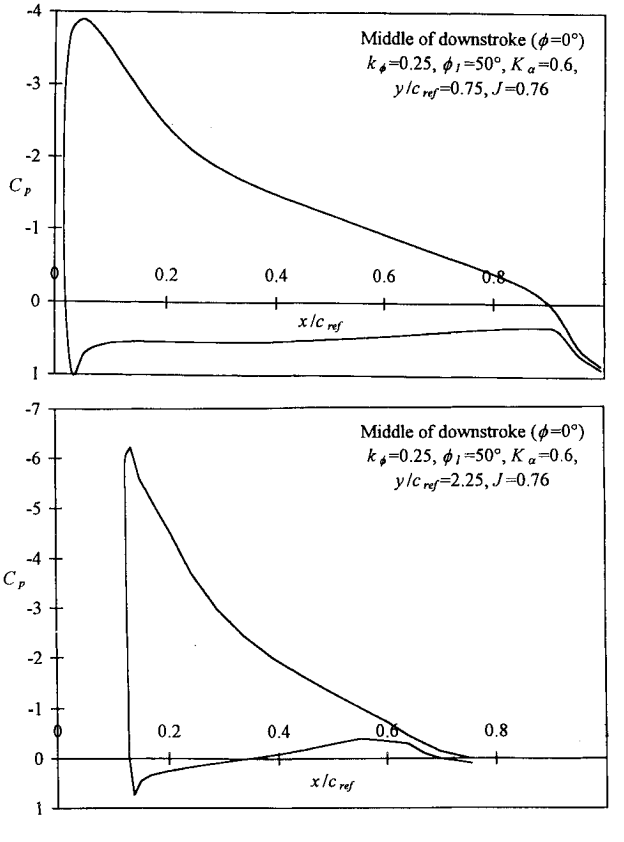

Fig. 10 Pressure distribution at one-fourth span and three-quarters span on pigeon wing with wing twist.

actually accelerating. The total flight efficiency would be decreased if the effects of form and separation drag were included. The wake for the wing in this flight configuration can be seen in Fig. 9.

The pressure distribution on the wing undergoing these twisting oscillations (Fig. 10) is much more reasonable that seen in the untwisted wing. The suction peak at the leading edge is much lower and most likely would not lead to flow separation. Based on the pressure distributions, geometric similarities to photographic analysis, and reasonable average loading over a flapping cycle, this motion is close to that experienced by a pigeon in this flight configuration.

Conclusions

A numerical tool was developed for the analysis of wings with time-dependent, deforming geometries. The present aerodynamic model is capable of computing the complex, unsteady flows of avian flight. As shown, this model simulated the flowfield characteristics of bird flight at much slower speeds than previous and current quasi-steady methods. Also, this model can be applied to investigate many other aspects of avian flight such as hovering, takeoff, or landing.

References

[1]Norberg, U. M., *Vertebrate Flight: Mechanics, Physiology, Morphology, Ecology, and Evolution*, Springer-Verlag, New York, 1990.

[2]Pennycuick, C. J., "Power Requirements for Horizontal Flight in the Pigeon Columbia Livia," *Journal of Experimental Biology*, Vol. 49, No. 3, 1968, pp. 527–555.

[3]Phlips, P. J., East, R. A., and Pratt, N. H., "An Unsteady Lifting Line Theory of Flapping Wings with Application to the Forward Flight of Birds," *Journal of Fluid Mechanics*, Vol. 112, Nov. 1981, pp. 97–125.

[4]DeLaurier, J. D., "An Aerodynamic Model for Flapping-Wing Flight," *Aeronautical Journal*, Vol. 97, April 1993, pp. 125–130.

[5]Rayner, J. M. V., "A Vortex Theory of Animal Flight," *Journal of Fluid Mechanics*, Vol. 91, Pt. 4, 1979, pp. 697–763.

[6]Katz, J., and Plotkin, A., *Low-Speed Aerodynamics: From Wing Theory to Panel Methods*, McGraw-Hill, San Francisco, CA, 1991.

[7]Spedding, G. R., "The Wake of a Jackdaw (Corvus Monedula) in Slow Flight," *Journal of Experimental Biology*, Vol. 125, Sept. 1986, pp. 287–307.

[8]Spedding, G. R., "The Wake of a Kestrel (Falco Tinnunculus) in Flapping Flight," *Journal of Experimental Biology*, Vol. 127, Jan. 1987, pp. 59–78.

[9]Richason, T. F., Katz, J., and Ashby, D. L., "Unsteady Panel Method for Flows with Multiple Bodies Moving Along Various Paths," AIAA Paper 93-0640, Jan. 1993.

[10]Yon, S., Katz, J., and Ashby, D. L., "Unsteady Fluid Dynamic Model for Propellor Induced Flow Fields," AIAA Paper 91-1664, June 1991.

[11]Archibald, F. S., "Unsteady Kutta Condition at High Values of the Reduced Frequency Parameter," *Journal of Aircraft*, Vol. 12, No. 6, 1975, pp. 545–550.

[12]Satyanarayana, B., and Davis, S., "Experimental Studies of Unsteady Trailing-Edge Conditions," *AIAA Journal*, Vol. 16, No. 2, 1978, pp. 125–129.

[13]Poling, D. R., and Telionis, D. P., "The Response of Airfoils to Periodic Disturbances—The Unsteady Kutta Condition," *AIAA Journal*, Vol. 24, No. 2, 1986, pp. 193–199.

[14]Giesing, J. P., "Nonlinear Two-Dimensional Unsteady Potential Flow with Lift," *Journal of Aircraft*, Vol. 5, No. 2, 1968, pp. 135–143.

[15]Giesing, J. P., "Vorticity and Kutta Condition for Unsteady Multienergy Flows," *Journal of Applied Mechanics*, Vol. 91, Series E, Sept. 1969, pp. 608–613.

[16]Basu, B. C., and Hancock, G. J., "The Unsteady Motion of a Two-Dimensional Aerofoil in Incompressible Inviscid Flow," *Journal of Fluid Mechanics*, Vol. 87, Pt. 1, 1978, pp. 159–178.

[17]Abbott, I. H., and von Doenhoff, A. E., *Theory of Wing Sections*, Dover, New York, 1959.

[18]Wagner, H., "Über die entstehung des dynamischen auftriebes von tragflügeln," *Zeitschrift fur Angewandte Mathematik und Mechanik*, Vol. 5, No. 1, 1925, pp. 17–35.

[19]Jones, R. T., "The Unsteady Lift of a Wing of Finite Aspect Ratio," NACA Rept. 681, April 1940.

[20]Fejtek, I., and Nehera, J., "Experimental Study of Flapping Wing Lift and Propulsion," *Aeronautical Journal*, Vol. 84, Jan. 1980, pp. 28–33.

[21]Nachtigall, W., and Wieser, J., "Profilmessugen am Taubenflügel," *Zeitschrift für vergleichende Physiologie*, Vol. 52, No. 4, 1966, pp. 333–346.

[22]Bilo, D., Lauck, A., and Nachtigall, W., "Measurements of Linear Body Accelerations and Calculations of the Instantaneous Aerodynamic Lift and Thrust in a Pigeon Flying in a Wind Tunnel," *Biona Report 3—Bird Flight—Vogelflug*, edited by W. Nachtigall, Gustav Fischer, Stuttgart, 1985, pp. 87–108.